Monthly Notices
of the
ROYAL ASTRONOMICAL SOCIETY

MNRAS **439,** 3121–3127 (2014)
Advance Access publication 2014 February 20

doi:10.1093/mnras/stu178

Dust grain growth and the formation of the extremely primitive star SDSS J102915+172927

Gen Chiaki,[1]★ Raffaella Schneider,[2] Takaya Nozawa,[3] Kazuyuki Omukai,[4] Marco Limongi,[2,3] Naoki Yoshida[1,3] and Alessandro Chieffi[5]

[1]*Department of Physics, Graduate School of Science, The University of Tokyo, 7-3-1 Hongo, Bunkyo, Tokyo 113-0033, Japan*
[2]*INAF/Osservatorio Astronomico di Roma, via Frascati 33, I-00040 Roma, Italy*
[3]*Kavli Institute for the Physics and Mathematics of the Universe (WPI), Todai Institutes for Advanced Study, The University of Tokyo, Kashiwa, Chiba 277-8583, Japan*
[4]*Astronomical Institute, Tohoku University, Sendai 980-8578, Japan*
[5]*INAF/IASF, Via Fosso del Cavaliere 100, I-00133 Roma, Italy*

Accepted 2014 January 22. Received 2014 January 22; in original form 2013 October 11

ABSTRACT

Dust grains in low-metallicity star-forming regions may be responsible for the formation of the first low-mass stars. The minimal conditions to activate dust-induced fragmentation require the gas to be pre-enriched above a critical dust-to-gas mass ratio $\mathcal{D}_{\rm cr} = [2.6–6.3] \times 10^{-9}$. The recently discovered Galactic halo star SDSS J102915+172927 has a stellar mass of $0.8\,{\rm M}_\odot$ and a metallicity of $Z \sim 4.5 \times 10^{-5}\,{\rm Z}_\odot$ and represents an optimal candidate for the dust-induced low-mass star formation. Indeed, the critical dust-to-gas mass ratio can be overcome provided that at least $0.4\,{\rm M}_\odot$ of dust condenses in Pop III supernova ejecta, allowing for moderate destruction by the reverse shock. Here, we show that grain growth during the collapse of the parent gas cloud is sufficiently rapid to activate dust cooling and fragmentation into low-mass stars, even if dust formation in the first supernovae is less efficient or strong dust destruction does occur. We find that carbon grains do not experience grain growth because at densities below $n_{\rm H} \sim 10^6\,{\rm cm}^{-3}$ carbon atoms are locked into CO molecules. Silicates and magnetite grains accrete gas-phase species in the density range $10^9 < n_{\rm H} < 10^{12}\,{\rm cm}^{-3}$, until their gas-phase abundance drops to zero, reaching condensation efficiencies ≈1. The corresponding increase in the dust-to-gas mass ratio allows dust-induced cooling and fragmentation to be activated at $10^{12} < n_{\rm H} < 10^{14}\,{\rm cm}^{-3}$, before the collapsing cloud becomes optically thick to continuum radiation.

Key words: stars: formation – stars: low-mass – stars: Population II – ISM: abundances – dust, extinction – galaxies: evolution.

1 INTRODUCTION

The physical conditions which enable the first low-mass and long-lived stars to form in the Universe is still a subject of debate (Karlsson, Bromm & Bland-Hawthorn 2013). Recent numerical simulations of primordial star formation suggest that the first stars could have a wide variety of masses (for a recent comprehensive review, see Greif et al. 2012; Bromm 2013; Hirano et al. 2014). Indeed, no evidence for the existence of primordial low-mass stars has been found in surveys of the Galactic halo and in nearby dwarfs (Beers & Christlieb 2005).

Once the first supernovae (SNe) explode and start to seed the gas with metals and dust grains, the physical properties of star-forming regions change (Bromm, Yoshida & Hernquist 2003; Chiaki, Yoshida & Kitayama 2013a). Low-metallicity gas can achieve larger cooling rates through additional molecular species (OH, CO, H_2O), fine-structure line cooling (mostly O I and C II), and thermal emission from dust grains (Omukai 2000; Bromm et al. 2001; Schneider et al. 2002; Omukai et al. 2005). The relative importance of these coolants depends on the density (time) regime during the collapse and on the initial metallicity and dust content of the collapsing core.

O I and C II fine-structure line cooling dominates the thermal evolution at $n_{\rm H} < 10^4\,{\rm cm}^{-3}$ until the transition from non local thermal equilibrium to local thermal equilibrium occurs and the cooling efficiency decreases. Bromm & Loeb (2003) and Frebel, Johnson

★ E-mail: gen.chiaki@utap.phys.s.u-tokyo.ac.jp

& Bromm (2007) have discussed the critical O and C abundances required to overcome the compressional heating rate and fragment the gas, $[C/H]_{cr} = -3.5$ and $[O/H]_{cr} = -3.05$. Given the typical gas temperatures and densities where line-induced fragmentation takes place, the associated Jeans-unstable fragment masses are still relatively large, $\geq 10\,M_\odot$ (Schneider et al. 2006; Safranek-Shrader, Milosavljevic & Bromm 2014).

A pervasive fragmentation mode that allows the formation of solar or sub-solar mass fragments is activated at higher gas densities $n_H \sim 10^{12}$–$10^{14}\,cm^{-3}$ where dust grains are collisionally excited and emit continuum radiation, thereby decreasing the gas temperature, T, until it becomes coupled with the dust temperature, or the gas becomes optically thick (Schneider et al. 2002). The efficiency of this physical process depends on the dust-to-gas mass ratio and on the total cross-section of the grains, with smaller grains providing a larger contribution to cooling (Schneider et al. 2006). Hence, the minimal conditions for dust-induced fragmentation have been expressed in terms of a minimal critical dust-to-gas mass ratio,

$$S\mathcal{D}_{cr} = 1.4 \times 10^{-3}\,cm^2\,g^{-1} \left(\frac{T}{10^3\,K}\right)^{-1/2} \left(\frac{n_H}{10^{12}\,cm^{-3}}\right)^{-1/2}, \quad (1)$$

where S is the total cross-section of dust grains per unit dust mass and the expression holds in the regime where dust cooling is effective; hence, grain temperatures are much lower than gas temperature. An extensive parameter-space exploration shows that $\mathcal{D}_{cr} \sim 4.4 \times 10^{-9}$ can be considered as a good representative value for the minimal dust enrichment required to activate dust-induced fragmentation (Schneider et al. 2012a).

The recently discovered Galactic halo star SDSS J102915+172927 represents a perfect candidate for dust-induced fragmentation (Klessen, Glover & Clark 2012; Schneider et al. 2012b). It has a stellar mass of $<0.8\,M_\odot$ and a metallicity of only $Z_{obs} = 4.5 \times 10^{-5}\,Z_\odot$, being the most chemically pristine star ever observed in the Universe (Caffau et al. 2011). Schneider et al. (2012b) investigate the origin of SDSS J102915+172927 by reconstructing the physical conditions of the parent cloud out of which the star had formed. They assume pre-enrichment of the gas with metals and dust released by primordial core-collapse SNe, allowing for the partial destruction of grains by the reverse shock. To simulate the physical conditions of the parent cloud of SDSS J102915+172927 at the onset of collapse, the resulting metal and dust yields are characterized by the initial depletion factor $f_{dep,0}$, defined to be the ratio of dust mass relative to the total mass of heavy elements and are rescaled to the total metallicity of SDSS J102915+172927 yielding an initial dust-to-gas mass ratio of $\mathcal{D}_0 = f_{dep,0} Z_{obs}$. Given these initial conditions, Schneider et al. (2012b) follow the thermal evolution of the collapsing clouds and find dust-induced fragmentation to be effective only in four out of the eight models considered. Not surprisingly, since both $f_{dep,0}$ and $\mathcal{D}_0$ are assumed to be constant during the course of the collapse, the successful models conform to the condition that $f_{dep,0} > 0.01$, that is $\mathcal{D}_0 > \mathcal{D}_{cr}$.

In a recent paper, Nozawa, Kozasa & Nomoto (2012) show that as the density in the collapsing cloud increases, dust grains can grow in mass by accreting metal species. Grain growth during the collapse is very efficient and the dust-to-gas mass ratio increases even for very small initial gas metallicity and depletion factor. Earlier, in Chiaki, Nozawa & Yoshida (2013b), we have studied the impact of grain growth on the thermal evolution of collapsing clouds. It is shown that even for small values of the initial depletion factor, $f_{dep,0} \approx 10^{-3}$, and for initial metallicities in the range $10^{-5.5}$–$10^{-4.5}\,Z_\odot$, grain growth enables us to activate dust cooling at densities $n_H \sim 10^{12}$–$10^{14}\,cm^{-3}$, thereby inducing fragmentation into low-mass clumps. However, the model is based on a few simplifying assumptions, such as the use of an average grain size as a proxy to the full grain size distribution and of a single dust species to dominate the total dust mass.

The aim of the present study is to investigate the implications that the process of grain growth may have on the formation of a low-mass star with a metallicity of $Z = 4.5 \times 10^{-5}\,Z_\odot$ such as SDSS J102915+172927. Starting from the same SN progenitor models and initial conditions as Schneider et al. (2012b), we take into account the modifications induced by grain growth on the size distribution of the grains to check whether conditions favourable to fragmentation can be met. A more systematic investigation of the parameter space, including different SN models and initial gas metallicities, will be presented in a forthcoming paper (Chiaki et al., in preparation).

2 METHOD

We base our calculation on a one-zone semi-analytical model that enables us to follow the thermal evolution of the collapsing cloud and the process of grain growth in a self-consistent way. Here, we describe the new features of the model required to implement the process of grain growth. For each dust species initially present in the collapsing cloud, we calculate the time evolution of condensation efficiency, f_{ij}, defined as the *number* fraction of nuclei of element j condensed into grains of species i. We assume that (i) grains are spherical particles and (ii) the rate is controlled by a single chemical species, referred to as the key species, which corresponds to the reactant with the least collisional frequency on the target.

Hence, the growth rate of a dust species i can be expressed as

$$\left(\frac{dr}{dt}\right)_i = \alpha_i \left(\frac{4\pi}{3} a_{i,0}^3\right) \left(\frac{kT}{2\pi m_{i1}}\right)^{1/2} n_{i1}(t), \quad (2)$$

where α_i is the sticking probability of a gas particle on to grains of species i, $a_{i,0}$ is the radius of a single monomer of species i in the condensed phase, and m_{i1} and n_{i1} are the mass and number density of the key species for grains of species i.[1] Note that the growth rate is independent of the grain radius. In this paper, we consider size distribution function $\varphi_i(r)$ for grains of species i. The function is normalized as $\int \varphi_i(r)\,dr = 1$, and thus the number density of dust i with radii between r and $r + dr$ is $n_i \varphi_i(r)\,dr$, where n_i is the total number density of dust grains i. Given the size distribution at the time t, we can calculate the condensation efficiency of grains. Condensation efficiency is obtained by integrating the size distribution as

$$f_{ij}(t) = f_{ij,0} \frac{\int r^3 \varphi_i(r)\,dr}{\int r^3 \varphi_{i,0}(r)\,dr}, \quad (3)$$

where the subscript '0' indicates the initial values.

As the collapse proceeds, equation (2) allows us to compute the time-dependent grain size distribution, dust mass, and depletion factor. In addition, we need to compute the condensation efficiencies f_{ij}, defined as the number fraction of element j condensed into dust species i. We solve the non-equilibrium chemistry of eight primordial elements H^+, e^-, H, H^-, H_2, D^+, D, and HD, and 19 heavy elements C^+, C, CH, CH_2, CO^+, CO, CO_2, O^+, O, OH^+,

[1] The subscript $i1$ denotes the key *chemical species* for grains of species i (e.g. Mg atoms or SiO molecules for Mg_2SiO_4 grains). We use a different subscript j to indicate *elements* (e.g. Mg, Si, and so on).

OH, H_2O^+, H_2O, H_3O^+, O_2^+, O_2, Si, SiO, and SiO_2. Silicon atoms and SiO molecules are oxidized mainly by OH molecules (Langer & Glassgold 1990).

We adopt the same initial conditions as Schneider et al. (2012b) to understand how grain growth may affect the resulting cloud fragmentation properties. In these models, dust species included are forsterite (Mg_2SiO_4), enstatite ($MgSiO_3$), magnetite (Fe_3O_4), amorphous carbon (C), silica (SiO_2), and alumina (Al_2O_3). Then, we assume that silicate (Mg_2SiO_4 and $MgSiO_3$) and silica grains grow when SiO and SiO_2 molecules stick to the grains, respectively. Dust temperature, dust continuum opacity, and cooling rate are calculated at each time using the time-dependent grain size distribution function on the basis of formulae of Schneider et al. (2006). The size bins have an initial width of 0.1 dex. The results are not significantly different from the ones obtained when the initial size bins are 0.01 dex width.

Additional features of the model, other than the part of grain growth, are the same as in the model used by Schneider et al. (2012b). The collapsing gas cloud has a total metallicity of $Z_{\rm obs} = 4.5 \times 10^{-5}\,{\rm Z}_\odot$, equal to the observed metallicity of SDSS J102915+172927. The initial metal and dust contents are taken from two different Population III SN models with progenitor masses and explosion energies selected to minimize the scatter between the theoretical yields and the observed ones. Despite its very low iron content, SDSS J102915+172927 shows an abundance pattern consistent with typical Galactic halo signatures and the best agreement is found for 20 and 35 $M_\odot$ progenitors with mass cuts, explosion energies, and ejected ^{56}Ni mass in the range of what is typically found for ordinary core-collapse SNe (Limongi & Chieffi 2012). Using these SN models as input for the dust nucleation model (Bianchi & Schneider 2007), they compute the mass, composition, and size distribution of dust grains released in the interstellar medium, after allowing for the partial destruction of the newly formed dust by the reverse shock. As is the same as Schneider et al. (2012b), for each progenitor mass, we consider a model where no dust destruction is assumed to take place (`norev`) and three additional models with increasing dust destruction efficiency by the reverse shock (`rev1`, `rev2`, and `rev3` models which correspond to circumstellar medium gas densities of 10^{-25}, 10^{-24}, and $10^{-23}\,{\rm g\,cm^{-3}}$, respectively). The initial depletion factors for each of these eight models, $f_{\rm dep,0}$, are 0.26, 0.045, 0.015, and 0.0057 for `norev`, `rev1`, `rev2`, and `rev3` models with $M_{\rm pr} = 20\,{\rm M}_\odot$, respectively, and 0.076, 0.0082, 0.0025, and 0.0010 for `norev`, `rev1`, `rev2`, and `rev3` models with $M_{\rm pr} = 35\,{\rm M}_\odot$, respectively.

3 RESULTS

In the left-hand panel of Fig. 1, we show the predicted temperature evolution of collapsing clouds for all the initial conditions (progenitor masses and $f_{\rm dep,0}$) considered in this paper. The points mark the state where fragmentation conditions are met (Schneider & Omukai 2010). Molecular cooling leads to a first temperature dip at intermediate densities $n \approx 10^7\,{\rm cm^{-3}}$ where gravitational fragmentation is expected to form relatively massive fragments, with tens of solar masses. At higher densities, $n > 10^{11}\,{\rm cm^{-3}}$, grain growth has a large effect on the thermal evolution of the clouds: all the models show that enhanced dust cooling leads to a rapid decrease in gas temperature and fragmentation into sub-solar mass fragments, independently of $f_{\rm dep,0}$. This is different from what was originally found by Schneider et al. (2012b) where dust cooling was unable to activate fragmentation for `rev2` and `rev3` models with $M_{\rm pr} = 20\,{\rm M}_\odot$, and `rev1`, `rev2`, and `rev3` models with $M_{\rm pr} = 35\,{\rm M}_\odot$, which did not satisfy the condition of equation (1). To better clarify the impact of grain growth, in the right-hand panel of Fig. 1, we compare the

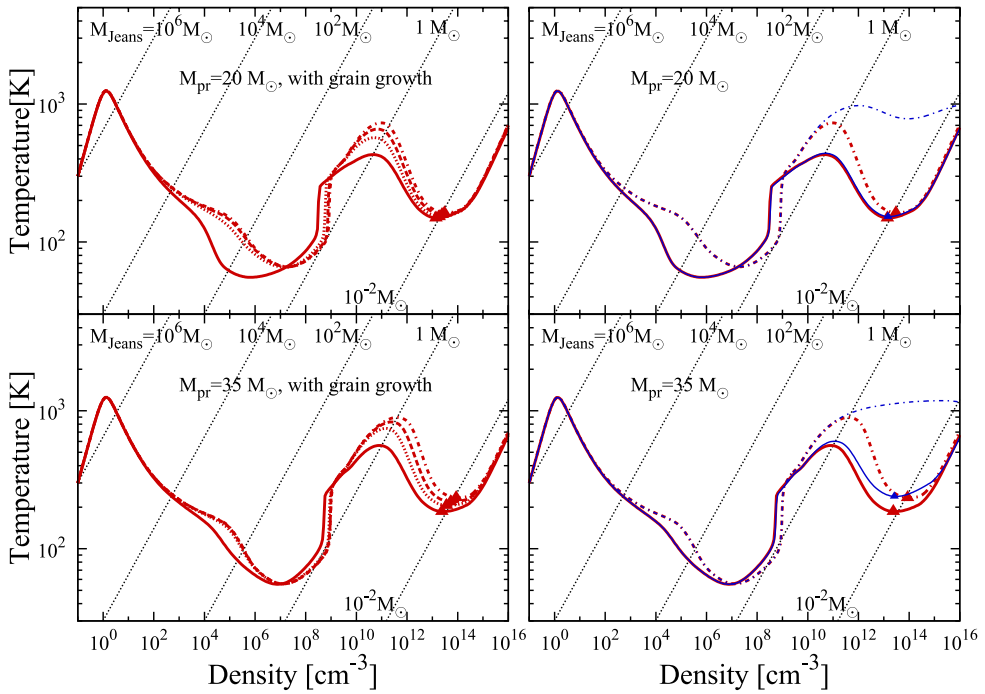

Figure 1. Left-hand panel: the temperature evolution for the `norev` (solid), `rev1` (dotted), `rev2` (dashed), and `rev3` (dot–dashed) models with grain growth for progenitor mass $M_{\rm pr} = 20\,{\rm M}_\odot$ (top) and $35\,{\rm M}_\odot$ (bottom) as a function of the cloud density. Right-hand panel: comparison between the temperature evolution with (red) and without (blue) grain growth. We plot the results for `norev` (solid) and `rev3` (dot–dashed) models. Triangles identify the states where the fragmentation conditions are met.

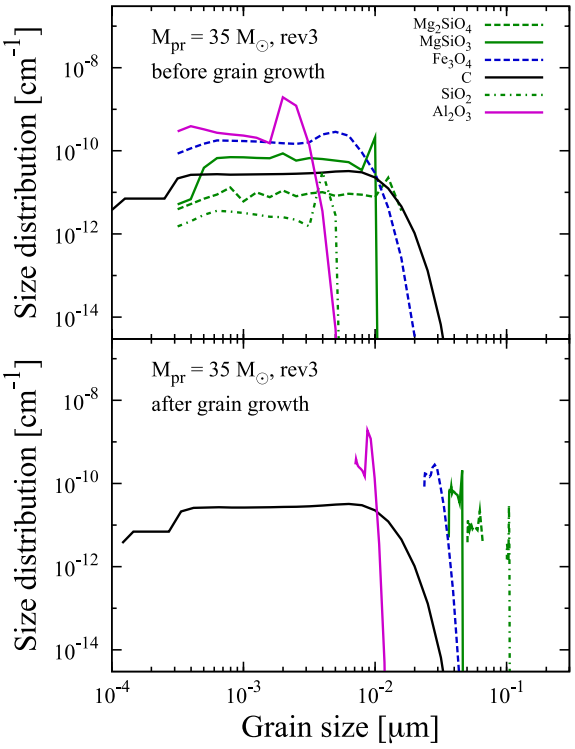

Figure 2. Size distribution functions, $n_i\varphi_i(r)/n_{\rm H}$, of different dust species before (top) and after (bottom) grain growth for the `rev3` model with $M_{\rm pr} = 35\,{\rm M}_\odot$.

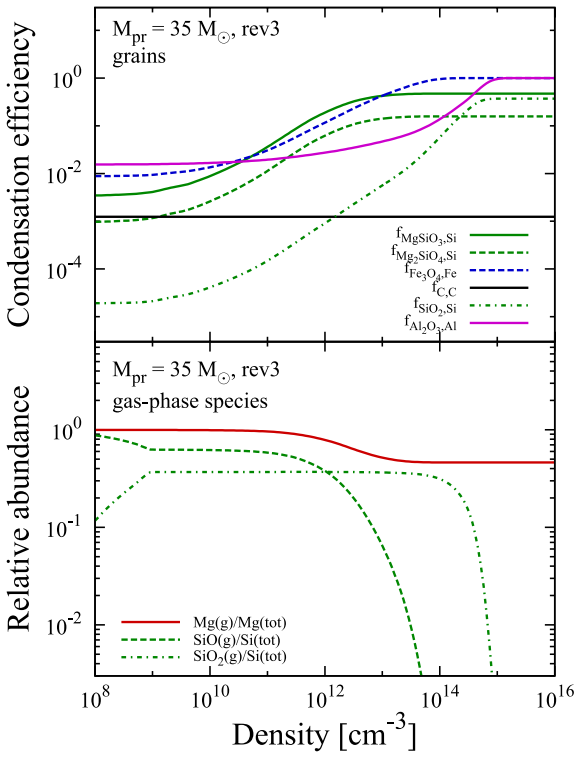

Figure 3. Top panel: the evolution of the condensation efficiency as a function of the cloud central density. Bottom panel: the relative abundance of gas-phase elements. Red solid curve represents the number fraction of gas-phase magnesium atom relative to total Mg nuclei. Green dashed and dot–dashed curves depict the number fraction of SiO and SiO_2 molecules relative to total Si nuclei, respectively.

thermal evolution of the `norev` and `rev3` models with and without grain growth.[2] At densities $n < 10^{11}\,{\rm cm}^{-3}$, the thermal tracks are still hardly affected by grain growth because dust cooling itself is not effective in this regime. The `norev` tracks appear to be only moderately affected because almost all refractory elements are already depleted (0.93 of Mg, 1.0 of Fe for $M_{\rm pr} = 20\,{\rm M}_\odot$) if they are not destroyed by the effects of reverse shocks. Conversely, the evolution of `rev3` models, which suffers the strongest dust destruction by the reverse shock and have very low initial depletion factors, show that grain growth leads to efficient cooling and fragmentation at $n > 10^{11}\,{\rm cm}^{-3}$, where the tracks strongly deviate from the cases without grain growth.

We first discuss the results for `rev3` model with $M_{\rm pr} = 35\,{\rm M}_\odot$. In Fig. 2, for each dust species we show the predicted grain size distribution functions, $n_i\varphi_i(r)/n_{\rm H}$, in unit of ${\rm cm}^{-1}$ before (upper panel at $n_{\rm H} = 0.1\,{\rm cm}^{-3}$) and after (bottom panel at $n_{\rm H} = 10^{16}\,{\rm cm}^{-3}$) grain growth. We can see that the radii of all grain species, except for carbon dust, increase. The size distribution of carbon grains is nearly unaffected because C atoms are already depleted into CO molecules early at densities below $n_{\rm H} \sim 10^6\,{\rm cm}^{-3}$. Since the growth rate, $({\rm d}r/{\rm d}t)_i$, is independent of grain radius (equation 2), the net effect is an overall shift of the size distribution function to larger radii. For the same model, we also show in Fig. 3 the evolution of the condensation efficiencies and the fractional abundance of gas-phase elements as a function of the cloud central density. As expected, the condensation efficiencies of carbon atoms remains constant and almost equal to its initial value. The first grain species to grow at $n_{\rm H} \sim 10^9$–$10^{12}\,{\rm cm}^{-3}$ are silicate (Mg_2SiO_4 and $MgSiO_3$, solid and dashed lines in the upper panel, respectively) grains whose key species is the SiO molecule. As silicate grains grow, the abundance of SiO molecules decreases until its abundance eventually drops to zero (see the dashed line in the bottom panel). The growth of silica grains is controlled by SiO_2 molecules whose formation rate grows with density. Though the abundance of SiO_2 molecules remains nearly constant because the abundance of SiO_2 grains are small at $n_{\rm H} \sim 10^9$–$10^{13}\,{\rm cm}^{-3}$, it eventually drops to zero (dot–dashed line in the bottom panel). The condensation efficiency of silicon atoms on to silica grains grows by more than four orders of magnitudes. Finally, although with different evolutionary properties, Fe and Al condensation efficiencies reach unity, meaning that all the available Al and Fe grains are condensed into solid grains.

We consider that grain growth is significant when the collapse has reached the density (time) threshold, $n_{{\rm grow},i}$, at which the condensation efficiency becomes 0.5. From the results of calculations, we find a fitting function of $n_{{\rm grow},i}$ as

$$n_{{\rm grow},i} = 1.0\times10^{12}\,{\rm cm}^{-3}\left(\frac{A_j}{7.1\times10^{-10}}\right)^{-2}\left(\frac{f_{ij,0}}{0.1}\right)^{-0.8} \times\left(\frac{r_{i,0}^{\rm grow}}{0.01\,\mu{\rm m}}\right)^{2}\left(\frac{a_{i,0}}{1\,\text{Å}}\right)^{-6}\left(\frac{m_{i1}}{m_{\rm H}}\right),$$

where $r_{i,0}^{\rm grow}$ is the mass-weighted average radius, $r_{i,0}^{\rm grow} = \langle r^3\rangle_{i,0}^{1/3}$. Hence, the condition for efficient grain growth depends on specific properties of the grain species as well as on the abundance of the key species. As an example, grains with larger $a_{i,0}$, such as silicates, grow earlier in the evolution (at lower densities), whereas in `rev3`

[2] Our calculations without grain growth are the same as the calculations performed by Schneider et al. (2012b).

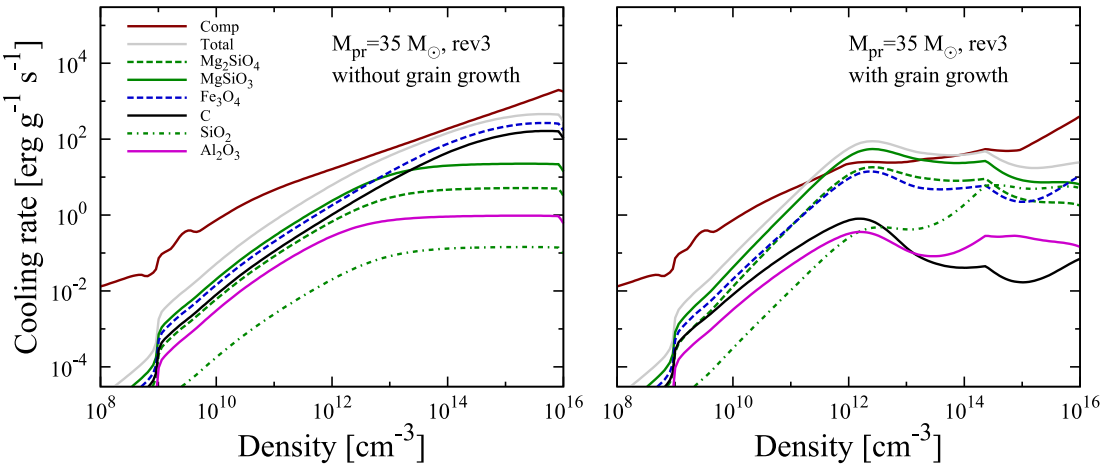

Figure 4. Compressional heating (red) and dust cooling rates as a function of gas density for `rev3` models with $M_{\rm pr} = 35\,{\rm M}_{\odot}$ with (left) and without (right) grain growth. Each line represents the contribution of a single dust species and the light grey solid line shows the total cooling rate. The abrupt change of slope at $n_{\rm H} \simeq 10^{14}\,{\rm cm}^{-3}$ is where to continuum opacity becomes effective.

model with $M_{\rm pr} = 35\,{\rm M}_{\odot}$, aluminium abundance is so small that the growth of Al_2O_3 grains is inefficient at all but the largest densities.

While the growth rate of each specific grain depends also on the initial composition of gas-phase elements, we find that grain growth is able to activate dust cooling and fragmentation for all the explored initial conditions (two SN progenitor models, a total gas metallicity set to reproduce the observed surface metallicity of SDSS J102915+172927, and $0.001 < f_{\rm dep,0} < 0.26$). In Fig. 4, we show the cooling rate for `rev3` models with $M_{\rm pr} = 35\,{\rm M}_{\odot}$, each line representing the contribution of a single dust species. Left-hand panel shows the result without grain growth. In this case, total dust cooling does not exceed gas compressional heating. This means that the gas does not meet the condition for fragmentation. With grain growth (right-hand panel), dust cooling is increased and dominates over compressional heating rate.

The dominant coolants are silicate and magnetite grains. Even if only $MgSiO_3$ grains are present, their effect on the cooling rate would be enough to overcome compressional heating and enable gas fragmentation. This conclusion is independent of the specific reverse shock model (the value of $f_{\rm dep,0}$) as silicates and magnetite grains always represent the dominant dust species. Compressional heating is smaller for the model with grain growth because the rate is proportional to temperature which is reduced by enhanced dust cooling. Cooling rates increase with density for $10^9\,{\rm cm}^{-3} < n_{\rm H} < 10^{12}\,{\rm cm}^{-3}$ as a consequence of the combined effects of grain growth and the increasing collisional rate between dust and gas particles. Above $n_{\rm H} \sim 10^{12}\,{\rm cm}^{-3}$, the cooling rates start to decline as the gas temperature approaches the dust temperature. For silicates and magnetite grains, this decrement is partly compensated by grain growth. At $n_{\rm H} \sim 10^{14}\,{\rm cm}^{-3}$, the gas cloud starts to be optically thick to continuum opacity.

4 DISCUSSION

The results discussed above have been obtained under the assumptions of a sticking probability of $\alpha_i = 1$ for all dust species. In addition, there may be physical mechanisms that limit grain growth, such as dust evaporation, and dust coagulation due to grain–grain collisions. However, none of these affects the gas fragmentation properties, at least in the models that we have investigated, as we explain in what follows.

We first consider the effect of a smaller sticking probability. In fact, the exact value of the sticking probability for each dust species is unknown. A more careful treatment might be required for grain species on to which more than one gas-phase element is accreted such as silicates. Let us assume that two elements, 1 and 2, are accreted on to a grain species i, with corresponding growth rates $({\rm d}r/{\rm d}t)_{i1}$ and $({\rm d}r/{\rm d}t)_{i2}$, respectively. If element 1 is the key species, then by definition, $({\rm d}r/{\rm d}t)_{i1} < ({\rm d}r/{\rm d}t)_{i2}$ and the growth rate of ith grains is set to be $({\rm d}r/{\rm d}t)_i = ({\rm d}r/{\rm d}t)_{i1}$. As long as $({\rm d}r/{\rm d}t)_{i1} < ({\rm d}r/{\rm d}t)_{i2}$, the sticking probability would not be affected by the species which collides with the second most frequent collision rate. However, when $({\rm d}r/{\rm d}t)_{i1} \sim ({\rm d}r/{\rm d}t)_{i2}$, element 2 collides less frequently and the sticking probability might be further reduced. We also run models assuming that $\alpha_i = 0.1$ for all dust species. In this conservative limit, dust formation in the SN ejecta is also affected and $f_{\rm dep,0}$ are further reduced with respect to the reference model. However, we find grain growth to be effective and the fragmentation condition to be verified for all progenitor and reverse shock models.

The effects of dust coagulation in star-forming clouds with different initial metallicities have been discussed by Hirashita & Omukai (2009). They show that as long as the grain velocities are governed by thermal motions, coagulation occurs at densities $n_{\rm H} > 10^7\,(Z/{\rm Z}_{\odot})^{-2}(T/100\,{\rm K})^{-1}\,{\rm cm}^{-3}$ but it does not have significant effects on the thermal evolution of clouds. In addition, grain growth increases the average grain mass, thereby decreasing their thermal velocity which eventually drops below the coagulation threshold velocity. Dust evaporation may be important if the dust temperature becomes comparable to the sublimation temperature. To check the importance of this effect, we have conservatively assumed that grains whose temperature is above the sublimation temperature are immediately returned to the gas phase. The sublimation temperatures as a function of density are taken from Pollack et al. (1994). We find that dust evaporation can be safely ignored because the dust temperature always remains well below the sublimation temperature for all the models which we investigate here.

5 CRITICAL INITIAL CONDITIONS FOR THE FORMATION OF SDSS J102915+172927

The results of the present study may have important implications for the formation of the first low-mass stars in the Universe.

Table 1. Critical abundances.

$M_{\rm pr}$ ($M_\odot$)	Model	$r^{\rm cool}_{\rm MgSiO_3}$ (μm)	$r^{\rm cool}_{\rm Fe_3O_4}$ (μm)	$f_{\rm MgSiO_3,Mg}$	$f_{\rm Fe_3O_4,Fe}$	$[{\rm Mg/H}]_{\rm cr}$	$[{\rm Fe/H}]_{\rm cr}$
20	`norev`	8.39e−03	2.38e−02	0.20	1.00	−5.02	−4.92
	`rev1`	1.57e−02	2.44e−02	0.35	0.43	−4.99	−4.53
	`rev2`	2.31e−02	2.55e−02	0.37	0.19	−4.84	−4.16
	`rev3`	3.27e−02	2.78e−02	0.40	0.07	−4.73	−3.70
		$r^{\rm cool}_{\rm MgSiO_3}$ (μm)	$r^{\rm cool}_{\rm Fe_3O_4}$ (μm)	$f_{\rm MgSiO_3,Si}$	$f_{\rm Fe_3O_4,Fe}$	$[{\rm Si/H}]_{\rm cr}$	$[{\rm Fe/H}]_{\rm cr}$
35	`norev`	1.45e−02	7.27e−03	0.60	1.00	−5.24	−5.43
	`rev1`	1.89e−02	1.01e−02	0.44	0.55	−4.99	−5.03
	`rev2`	2.51e−02	1.19e−02	0.32	0.28	−4.72	−4.66
	`rev3`	3.24e−02	1.43e−02	0.19	0.12	−4.39	−4.21

Note. We calculate the critical abundances of Si or Mg, and Fe (seventh and eighth columns, respectively) by using values obtained from our calculations at $n_{\rm H} = 10^{12}\,{\rm cm^{-3}}$ (third to sixth columns).

A smaller dust-to-gas mass ratio may be sufficient to activate dust-induced fragmentation by the accretion of heavy elements on to grains during cloud collapse. In particular, our analysis shows that the dust species that dominate cooling are silicates and magnetite. Grain growth do not affect carbon grains, even if these are initially present, because carbon atoms are rapidly locked into CO molecules during the first stages of the collapse. Hence, the conditions for low-mass star formation may rely on the initial abundance of other refractory elements, such as key elements of silicates and magnetite: Mg and Fe for our $M_{\rm pr} = 20\,{\rm M_\odot}$ models, and Si and Fe for our $M_{\rm pr} = 35\,{\rm M_\odot}$ models.

A conservative lower limit to the initial abundance of refractory elements can be obtained as follows. The critical condition expressed by equation (1) depends on the product of the dust-to-gas mass ratio and the grain cross-section per unit mass of dust. If we assume a *single* dominant grain species i, the critical condition *after grain growth* can be written as

$$S\mathcal{D} = X_{\rm H} A_j f_{ij} \mu_i \frac{\pi \langle r^2 \rangle_i}{(4\pi/3) s_i \langle r^3 \rangle_i} \geq S\mathcal{D}_{\rm cr}, \quad (4)$$

where s_i is the material density of grains i. Here, we define another characteristic size for dust cooling as $r_i^{\rm cool} = \langle r^3 \rangle_i / \langle r^2 \rangle_i$. From equation (4), the critical abundance reads

$$A_{j,{\rm cr}} = 1.4 \times 10^{-3} \frac{4\, s_i\, r_i^{\rm cool}}{3 X_{\rm H}\, f_{ij}\, \mu_i} \left(\frac{T}{10^3\,{\rm K}} \right)^{-1/2} \left(\frac{n_{\rm H}}{10^{12}\,{\rm cm^{-3}}} \right)^{-1/2},$$

for $(i, j) = ({\rm MgSiO_3}, {\rm Si\ or\ Mg})$ and $({\rm Fe_3O_4}, {\rm Fe})$, respectively. Table 1 shows the critical abundances that correspond to the values of $r_i^{\rm cool}$ and f_{ij} at $n_{\rm H} = 10^{12}\,{\rm cm^{-3}}$, obtained for each of the SN model that we have explored. Given the large variation of condensation efficiencies experienced by the key elements in the different models, we can take as indicative critical abundances the maximum and minimum values that we find for each refractory element: $[{\rm Mg/H}]_{\rm cr} = [-5.02: -4.73]$, $[{\rm Si/H}]_{\rm cr} = [-5.24: -4.73]$, and $[{\rm Fe/H}]_{\rm cr} = [-5.43: -3.70]$, where we have normalized to solar abundances.[3]

The initial abundances of Mg, Si, and Fe predicted by the initial SN progenitors are $[{\rm Mg/H}] = -4.02$ and $[{\rm Fe/H}] = -4.55$ for the $M_{\rm pr} = 20\,{\rm M_\odot}$ models and $[{\rm Si/H}] = -4.39$ and $[{\rm Fe/H}] = -4.71$ for the $M_{\rm pr} = 35\,{\rm M_\odot}$ models with $Z = 4.5 \times 10^{-5}\,{\rm Z_\odot}$. Hence, for all our models, the Si or Mg abundances are sufficient or marginally sufficient (for `rev3` model with $M_{\rm pr} = 35\,{\rm M_\odot}$) to enable fragmentation even if there were (hypothetically) only $MgSiO_3$ grains in the clouds. Conversely, in all models but the `rev1` model with $M_{\rm pr} = 35\,{\rm M_\odot}$, the Fe abundance is not sufficient to enable fragmentation if only Fe_3O_4 grains are present in the clouds. These conclusions are consistent with the results obtained by the full calculations shown in Fig. 1 and in the right-hand panel of Fig. 4.

Recently, Ji, Frebel & Bromm (2014) have compared critical silicate abundances for dust cooling to chemical abundances of metal-poor stars, with $[{\rm Fe/H}] < -4$. Assuming silicon-based dust with different grain size distributions, they conclude that, out of the nine stars considered, two to four stars show silicate abundances below the critical ones, pointing to a different formation pathway. Interestingly enough, all the stars that cannot form through silicon-based dust satisfy the criterion for O I and C II fine-structure line cooling (Frebel et al. 2007).

We conclude that low-mass star formation induced by dust cooling may be more common than previously thought based on the required initial dust-to-gas mass ratio of very low-metallicity star-forming clouds. Although the first SNe may already provide enough dust grains, our study – which is motivated by the observed properties of SDSS J102915+172927– suggests that even in the extreme conditions where a large fraction of the newly formed dust is destroyed by the reverse shock of the SN, grain growth during the collapse is able to replenish the required amount of dust provided that a minimum abundance of refractory elements (mostly Si, Fe, and Mg) is initially present in the gas phase.

ACKNOWLEDGEMENTS

We thank Simone Bianchi for his kind collaboration. GC is supported by Research Fellowships of the Japan Society for the Promotion of Science (JSPS) for Young Scientists. This work is supported by World Premier International Research Center Initiative (WPI Initiative), MEXT, Japan, and in part by grant-in-aid for Scientific Research from the JSPS Promotion of Science (23540324, 25287040, 22684004, and 23224004). The research leading to these results has received funding from the European Research Council under the European Union's Seventh Framework Programme (FP/2007-2013) / ERC Grant Agreement no. 306476.

[3] We have considered $A_{\rm Fe,\odot} = 3.31 \times 10^{-5}$, $A_{\rm Si,\odot} = 3.31 \times 10^{-5}$, and $A_{\rm Mg,\odot} = 3.47 \times 10^{-5}$ (Caffau et al. 2011). Also, the mean molecular weights per unit key elements are $\mu_{\rm MgSiO_3} = 100$ and $\mu_{\rm Fe_3O_4} = 77.3$. The material densities are $s_{\rm MgSiO_3} = 3.21\ {\rm g\ cm^{-3}}$ and $s_{\rm Fe_3O_4} = 5.25\ {\rm g\ cm^{-3}}$ (Nozawa et al. 2003).

REFERENCES

Beers T. C., Christlieb N., 2005, ARA&A, 43, 531
Bianchi S., Schneider R., 2007, MNRAS, 378, 973
Bromm V., 2013, Rep. Prog. Phys., 76, 112901
Bromm V., Loeb A., 2003, Nature, 425, 812
Bromm V., Ferrara A., Coppi P. S., Larson R. B., 2001, MNRAS, 328, 969
Bromm V., Yoshida N., Hernquist L., 2003, ApJ, 596, L135
Caffau E. et al., 2011, Nature, 477, 67
Chiaki G., Yoshida N., Kitayama T., 2013a, ApJ, 762, 50
Chiaki G., Nozawa T., Yoshida N., 2013b, ApJ, 765, L3
Frebel A., Johnson J. L., Bromm V., 2007, MNRAS, 380, L40
Greif T. H., Bromm V., Clark P. C., Glover S. C. O., Smith R. J., Klessen R. S., Yoshida N., Springel V., 2012, MNRAS, 424, 399
Hirano S., Hosokawa T., Yoshida N., Umeda H., Omukai K., Chiaki G., Yorke H. W., 2014, ApJ, 781, 60
Hirashita H., Omukai K., 2009, MNRAS, 399, 1795
Ji A. P., Frebel A., Bromm V., 2014, ApJ, 782, 95
Karlsson T., Bromm V., Bland-Hawthorn J., 2013, Rev. Mod. Phys., 85, 809
Klessen R. S., Glover S. C. O., Clark P. C., 2012, MNRAS, 421, 3217
Langer W. D., Glassgold A. E., 1990, ApJ, 352, 123
Limongi M., Chieffi A., 2012, ApJS, 199, 38
Nozawa T., Kozasa T., Umeda H., Maeda K., Nomoto K., 2003, ApJ, 598, 785
Nozawa T., Kozasa T., Nomoto K., 2012, ApJ, 756, L35
Omukai K., 2000, ApJ, 534, 809
Omukai K., Tsuribe T., Schneider R., Ferrara A., 2005, ApJ, 626, 627
Pollack J. B., Hollenbach D., Beckwith S., Simonelli D. P., Roush T., Fong W., 1994, ApJ, 421, 615
Safranek-Shrader C., Milosavljevic M., Bromm V., 2014, MNRAS, 438, 1669
Schneider R., Omukai K., 2010, MNRAS, 402, 429
Schneider R., Ferrara A., Natarajan P., Omukai K., 2002, ApJ, 571, 30
Schneider R., Omukai K., Inoue A. K., Ferrara A., 2006, MNRAS, 369, 1437
Schneider R., Omukai K., Bianchi S., Valiante R., 2012a, MNRAS, 419, 1566
Schneider R., Omukai K., Limongi M., Ferrara A., Salvaterra R., Chieffi A., Bianchi S., 2012b, MNRAS, 423, L60

This paper has been typeset from a TEX/LATEX file prepared by the author.